Article:
Stuart, M.B., Davies, M., Fisk, C. et al. (5 more authors) (2024) Smartphone-based hyperspectral imaging for ice sheet and proglacial applications in South-West Greenland. Science of The Total Environment, 951. 175516. ISSN 0048-9697

https://doi.org/10.1016/j.scitotenv.2024.175516

Science of the Total Environment 951 (2024) 175516

Contents lists available at ScienceDirect

Science of the Total Environment

journal homepage: www.elsevier.com/locate/scitotenv

Smartphone-based hyperspectral imaging for ice sheet and proglacial applications in South-West Greenland

M.B. Stuart [a,*], M. Davies [b], C. Fisk [b], E. Allen [c], A.J. Sole [d], R. Ing [e], M.J. Hobbs [b], J.R. Willmott [b]

[a] College of Science and Engineering, University of Derby, Derby DE22 1GB, UK
[b] Department of Electronic & Electrical Engineering, University of Sheffield, Sheffield S1 4ET, UK
[c] PyrOptik Instruments Ltd, The Innovation Centre, Sheffield S1 4DP, UK
[d] Department of Geography, University of Sheffield, Sheffield S10 2TN, UK
[e] School of Geosciences, University of Edinburgh, Edinburgh EH8 9XP, UK

HIGHLIGHTS

- A low-cost approach to in-field spectral data collection in extreme environments
- Smartphone-based instrumentation enables rapid and accurate data collection
- On ice measurements successfully incorporated into ice surface energy balance model
- Proglacial measurements highlight potential for vegetation and lichen-based studies
- Machine learning provides accurate automatic identification of spectral targets

GRAPHICAL ABSTRACT

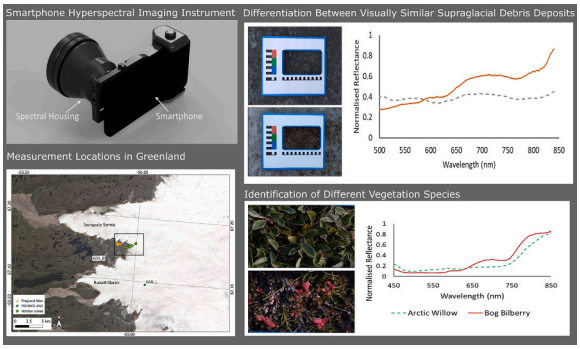

ARTICLE INFO

Editor: Jay Gan

Keywords:
Hyperspectral
Smartphone
Low-cost
Greenland ice sheet
Field deployment
Environmental monitoring

ABSTRACT

Hyperspectral imaging is a valuable analytical technique with significant benefits for environmental monitoring. However, the application of these technologies remains limited, largely by the cost and bulk associated with available instrumentation. This results in a lack of high-resolution data from more challenging and extreme environmental settings, limiting our knowledge and understanding of the effects of climate change in these regions. In this article we challenge these limitations through the application of a low-cost, smartphone-based hyperspectral imaging instrument to measurement and monitoring activities at the Greenland Ice Sheet. Datasets are captured across a variety of supraglacial and proglacial locations covering visible and near infrared wavelengths. Our results are comparable to the existing literature, despite being captured with instrumentation costing over an order of magnitude less than currently available commercial technologies. Practicalities for field deployment are also explored, demonstrating our approach to be a valuable addition to the research field with the potential to improve the availability of datasets from across the cryosphere, unlocking a wealth of data collection opportunities that were hitherto infeasible.

* Corresponding author at: College of Science and Engineering, University of Derby, Derby DE22 1GB, UK.
E-mail address: m.stuart@derby.ac.uk (M.B. Stuart).

https://doi.org/10.1016/j.scitotenv.2024.175516
Received 22 May 2024; Received in revised form 9 August 2024; Accepted 12 August 2024
Available online 13 August 2024

1. Introduction

Hyperspectral imaging is a highly versatile analytical technique with potential for a wide variety of applications within environmental monitoring (Aasen et al., 2015; Näsi et al., 2015; Stuart et al., 2019; Jia et al., 2020; Rodrigues and Hemmer, 2022). By providing a rapid, non-destructive, and information-rich form of data collection, it enables real-time monitoring and decision making across a broad range of locations and measurement scenarios, reducing the need for time-consuming and often complex sample collection and logistics associated with the reliable transport of representative samples for further testing. The non-invasive analysis offered by hyperspectral imaging techniques enables samples to be analysed in their true in-situ state. This is of considerable importance in the context of the ongoing climate crisis where detailed datasets are required to enable us to better understand the effects of climatic changes. However, despite these significant benefits, the application of hyperspectral imaging techniques within these contexts remains comparatively limited to applications in other disciplines. This is largely due to the high costs and low portability typically associated with these instruments, limiting their application to better-resourced research teams across more easily accessible locations. The monitoring of more extreme environmental settings is particularly affected by these restrictions, significantly limiting the data collection opportunities across these typically more inaccessible areas (O'Neal, 2010). These restrictions, therefore, have a compounding effect on our understanding within climate-critical environments, limiting our knowledge to a comparatively small group of accessible locations (O'Neal, 2010; Stuart et al., 2019). Our research seeks to address these restrictions by improving the democratisation of hyperspectral imaging applications within more challenging and difficult to access areas.

Applications of hyperspectral imaging within the cryosphere are a key component for the accurate monitoring of climate-critical environments, particularly the identification and monitoring of light absorbing impurities (LAIs) across glacier ice and snow. These particles have a significant impact on albedo and radiative forcing, and thus play an important role in melt dynamics within the cryosphere (Warren, 2019). Traditional approaches to monitoring LAI typically utilise portable multispectral imaging instruments and/or satellite-based analyses (Painter et al., 2001; Casey and Kääb, 2012; Di Mauro et al., 2015; Naegeli et al., 2015; Cook et al., 2017a; Cook et al., 2017b). However, the spectral and spatial resolution limitations associated with these techniques, combined with the high spectral similarities present between LAI species, make it difficult to accurately identify LAI within glacial settings (Seager et al., 2005; Cook et al., 2017a). Whilst some studies have successfully identified LAI using these techniques, such as Wang et al. (2020) who detected algal blooms using satellite imagery, it remains difficult due to current limitations. LAI typically found across glacial environments such as windblown and englacially transported mineral dusts, and algal blooms have typically similar spectral profiles that result in decreased reflectance, particularly across visible wavelengths. Whilst slight spectral variations mean that they can be differentiated, e.g. an increase in reflectance across red wavelengths (ca. 625–740 nm) typically associated with mineral dusts (Dumont et al., 2014; Zhang et al., 2017), and the presence of absorption features that indicate the presence of chlorophyll *a* in algal blooms (Painter et al., 2001; Cook et al., 2017a), these features are often missed by measurements with coarser banding. Hyperspectral imaging provides a means of overcoming these limitations and has been previously applied in several studies, demonstrating that it can accurately identify subtle variations in spectral response between LAIs (Di Mauro et al., 2017; Cook et al., 2017a; Stuart et al., 2019; Williamson et al., 2019; Halbach et al., 2023).

In proglacial environments, hyperspectral imaging can provide detailed observations of lichen and vegetation communities, enabling more thorough analysis of community health and increasing the ease of species identification. Application of hyperspectral approaches in these settings aids traditional field observations, creating reliable visual records for future comparisons. This, in turn, reduces the time required for detailed on-site analyses, easing pressure on time-critical field studies. Existing applications of spectral imaging in these settings have shown considerable promise (Van der Veen and Csatho, 2005; Salehi et al., 2016; Guedes et al., 2022), suggesting that if hyperspectral data could be collected more widely, more detailed and reliable data analysis could be achieved in these settings.

In this article we demonstrate the effectiveness of a portable, low-cost alternative to currently available instrumentation. We apply the Hyperspectral Smartphone, a low-cost smartphone-based hyperspectral imaging instrument, to data collection scenarios across supraglacial and proglacial locations at Isunguata Sermia, south-west Greenland. Using this instrumentation, we capture datasets across visible and near infrared (NIR) wavelengths (450 nm – 850 nm). Datasets are acquired from a variety of features, with the aim of highlighting the significant potential offered by low-cost hyperspectral imaging instruments within these contexts. Machine learning image segmentation is applied to the captured datasets to demonstrate the significant data analysis opportunities provided through these novel approaches. By providing a highly portable, low-cost alternative to currently available instrumentation, we aim to open-the-door for more detailed spectral analysis studies within extreme and difficult to access environments.

2. Methodology

2.1. Field site

The study area in south-west Greenland (67.150° N, 50.040° W) included both ice-covered and proglacial areas, close to the ice sheet margin. Fig. 1(A) shows the location of the study area in south-west Greenland. Fig. 1(B) and 1(C) show the context of the study site close to Isunnguata Sermia and the location of proglacial and supraglacial measurement sites respectively. This region features a slow-moving ice margin with average winter speeds of 20–100 m yr^{-1} recorded at Isunguata Sermia, where ice flows in an east-west orientation (Jones et al., 2018; Derkacheva et al., 2021). The climate in this area is defined as low Arctic, experiencing average highs of 16 °C in summer and average lows of −24 °C in winter (Lindbäck and Pettersson, 2015). The dominant source of LAI within this area is local windblown dust due to the study site's proximity to the ice margin (Wientjes et al., 2011). Located directly north of Russell Glacier, this region represents one of the most studied areas of the Greenland Ice Sheet (GrIS) (Lindbäck and Pettersson, 2015; Derkacheva et al., 2021; Harper et al., 2021), with a broad range of existing studies covering glacial and geophysical processes (e.g. Bartholomew et al., 2011; Palmer et al., 2011; Van De Wal et al., 2012; Sole et al., 2013; Wright et al., 2016; Yde et al., 2018; Maier et al., 2019; Derkacheva et al., 2021). A number of automatic weather stations (AWS), run by PROMICE, also cover this area (Fausto et al., 2021), providing valuable context for new device demonstration and testing. Measurements were completed across a two-week period between the 7th and 22nd August 2023 across supraglacial areas in the ablation zone of Isunguata Sermia and proglacial locations extending ca. 1 km from the ice margin.

2.2. Instrumentation

The Hyperspectral Smartphone (Fig. 2) is a low-cost, field portable hyperspectral imaging instrument. As outlined in Stuart et al. (2021) and Davies et al. (2022), the Hyperspectral Smartphone uses a 3-D printed spectral housing to enable hyperspectral datasets to be captured with a smartphone camera. This instrument is now undergoing further development for commercialisation. In previous publications (Stuart et al., 2021; Davies et al., 2022; Stuart et al., 2022a) we have applied this instrument using an unmodified smartphone camera, enabling datasets to be captured across visible wavelengths. However, in this article we utilise a modified design enabling the spectral range of

the instrument to be extended into the near infrared (NIR). In the modified design, the infrared filter has been removed and the optics recalibrated to ensure visual focus was not impacted.

Table 1 shows the specifications used for the instrument. The smartphone used in this design represents a typical off-the-shelf handset. This particular handset was chosen for its affordability and popularity within commercial markets, highlighting the quality of hyperspectral data collection that can be acquired with low-cost, off-the-shelf components. This instrument is a pushbroom-style hyperspectral instrument, where a line of spectral information is recorded per exposure as the instrument is translated across a scene (Stuart et al., 2019). At present this instrument is handheld; however, there is significant potential for drone-based applications in the future. The instrument provides a pixel resolution of typically 900 × 720 px but the width of the images is determined by the duration of the scan so this figure can vary.

To enable reliable measurements that remained unaffected by saturation, neutral density (ND) filters were fitted to reduce the intensity of reflected solar radiation. The Samsung Galaxy S9 provided greater user input, allowing the operator to manually adjust shutter speed reducing the required optical density of the external filters. The ND filters can be changed to suit illumination conditions.

2.3. Data collection and analysis

Measurements were captured across 21 sites in a catchment of Isunguata Sermia. To reduce the potential impact of illumination variations, all datasets were captured on clear sky or fully overcast days within 2 h of solar noon (Cook et al., 2017b). Hyperspectral measurements were acquired using the handheld method described in Davies et al. (2022), where an in-scene reference card is used to enable spatial and spectral corrections without the need for additional data collection. Standard RGB photographs were also captured for each location to provide a visual comparison to the hyperspectral datasets.

A test card (Fig. 3) with known spectral responses was imaged before data capture at each site, acting as a calibrated standard to ensure robust datasets were acquired. This allowed the accuracy of spectral datasets to be assessed in the field without the need for on-site spectral calibration. Additionally, a minimum of five scene passes were captured of each target to monitor the repeatability of captured datasets. Supraglacial measurements were captured for a variety of debris-laden and clean ice

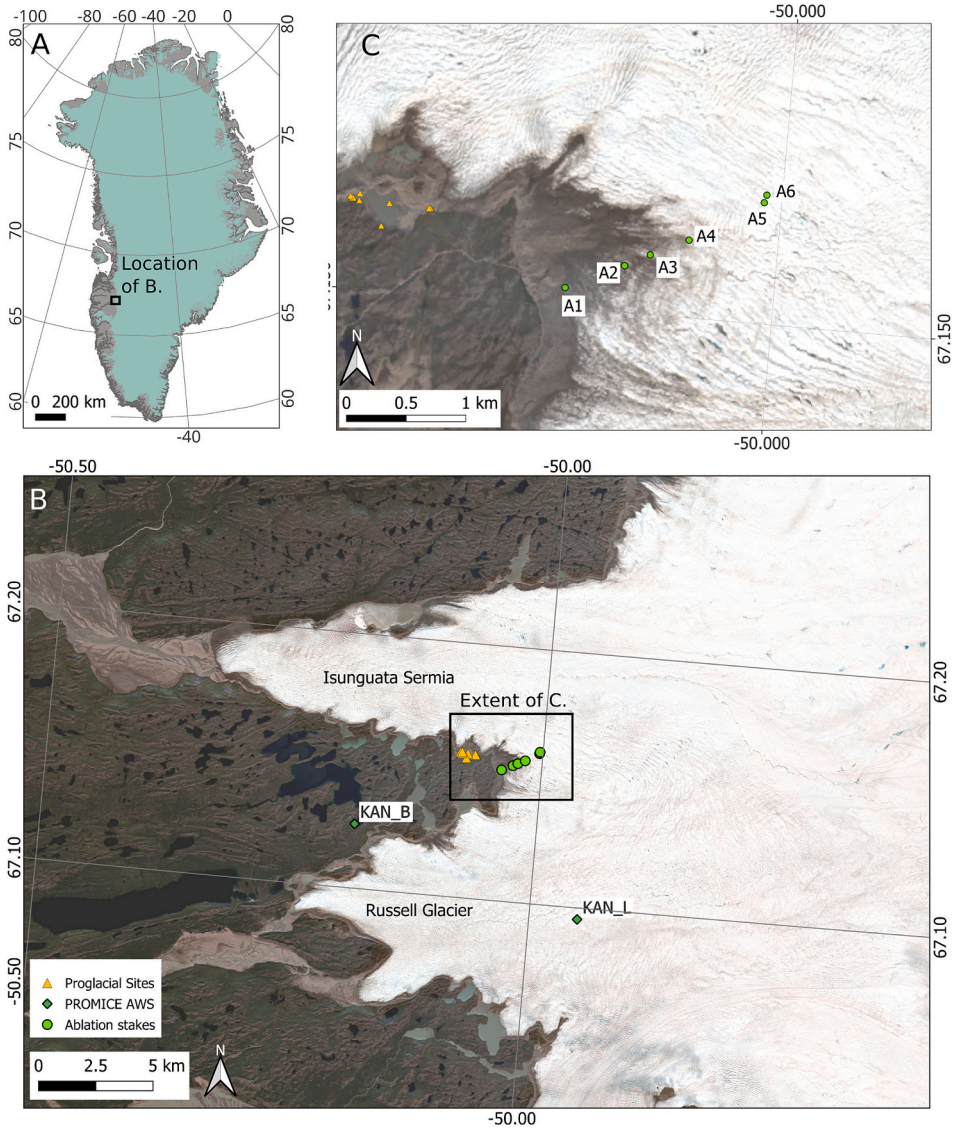

Fig. 1. Study area location in south-west Greenland (A). Context of study site close to Isunguata Sermia (B). Location of proglacial and supraglacial measurement sites on the south-eastern part of the tongue of Isunguata Sermia (C). Background image taken from Sentinel-2 L1C true colour image (Red = Band 4, Green = Band 3, Blue = Band 2) captured on 27th July 2023.

locations, whereas proglacial measurements were more varied covering lichen and shrub vegetation populations as well as a range of glacially and fluvially deposited clasts. Sites were chosen for their spectral and spatial diversity, giving us the opportunity to test the abilities of these low-cost instruments across a broad range of glaciologically relevant applications.

Whilst measurement quality was initially assessed in the field, post-processing and analysis were predominantly completed in the laboratory. Hyperspectral data cubes were built within MATLAB (R2023a) where spectral datasets were also corrected for sensor and illumination biases using white and dark references. The white reference was taken from the in-scene reference card, providing a distinct matte white reference for each measurement. This helped to account for variations in illumination that may have occurred between individual measurements. Furthermore, prior to their application in the field, these instruments were spectrally calibrated using a mercury argon lamp that produced a series of intense narrow peaks at known wavelengths. The peaks at 546.07 nm and 576.96 nm were used to calculate the wavelength range and spectral resolution. Further details on post-processing can be found in Davies et al. (2022).

In this article the terms "reflectance" and "albedo" are used regularly. To prevent confusion, in the context of this article we define these terms as follows: "reflectance" refers to the spectral reflectance of a target as a function of wavelength. "Albedo" refers to the reflective properties of a target and is used when discussing the fraction of light that is reflected from a target surface.

2.4. Machine learning

The data collected from the field was split into two sets, one for training and the other for testing. The training datasets were manually segmented. The machine learning was performed using MATLAB (R2023a) to read in manually labelled spectral data sets to train and produce a model to segment further data sets. The function "fitcnet" was used with default parameters to build the convolution neural network model, which could then be implemented using the "predict" function with the model and a spectral data cube from the testing dataset as the input. The use of this neural network function is precedented as an analysis tool (Slightam and Griego, 2023; Patmanee et al., 2024). The function applied the model to each of the spectra of the data cube and was given a score for each feature the model was trained to identify. The feature category given the highest score was assumed by the function to be the feature in question and an image was produced with highlighted areas corresponding to the presence of the feature/target. The final output was an overlay of the detected feature over a pseudo RGB image produced from the data cube where the spectrum corresponding to each pixel had been run through the function.

Table 1
Instrument Specifications.

	Instrument
Smartphone Handset	Samsung Galaxy S9
Imaging Mode	Pushbroom
Exposure Time (ms)	30
Spectral Range (nm)	450–850
Spectral Resolution (nm)	10
ND Filter Optical Density	1.6 Visible, 0.7 NIR
Weight (g)	301.64
Dimensions (cm)	14.5 × 8 × 9.5

2.5. Sample analysis

Several small samples of supraglacial debris were collected to undergo laboratory analysis for ground truthing (Table 2). These samples were stored at ambient temperature in plastic containers prior to measurements in the laboratory using a laboratory-based hyperspectral imaging instrument. Measurements were captured using the low-cost design discussed in Stuart et al. (2022b), covering a wavelength range of 450–750 nm. Illumination was provided by a Halogen lamp and the spectral characteristics of the light source were removed with a white correction in the same way that illumination bias was removed from the hyperspectral images captured in the field, ensuring a fair comparison between the two instruments. Samples were misted with water prior to measurements to better represent their in-situ state. These samples were used as ground truths to provide a reference to quantify the accuracy of the field portable instrumentation. Sediment descriptions in Table 2 are

Fig. 2. The Hyperspectral Smartphone. 3-D render of the instrument highlighting key components (left) and a photograph of the instruments in the field demonstrating their high portability (right).

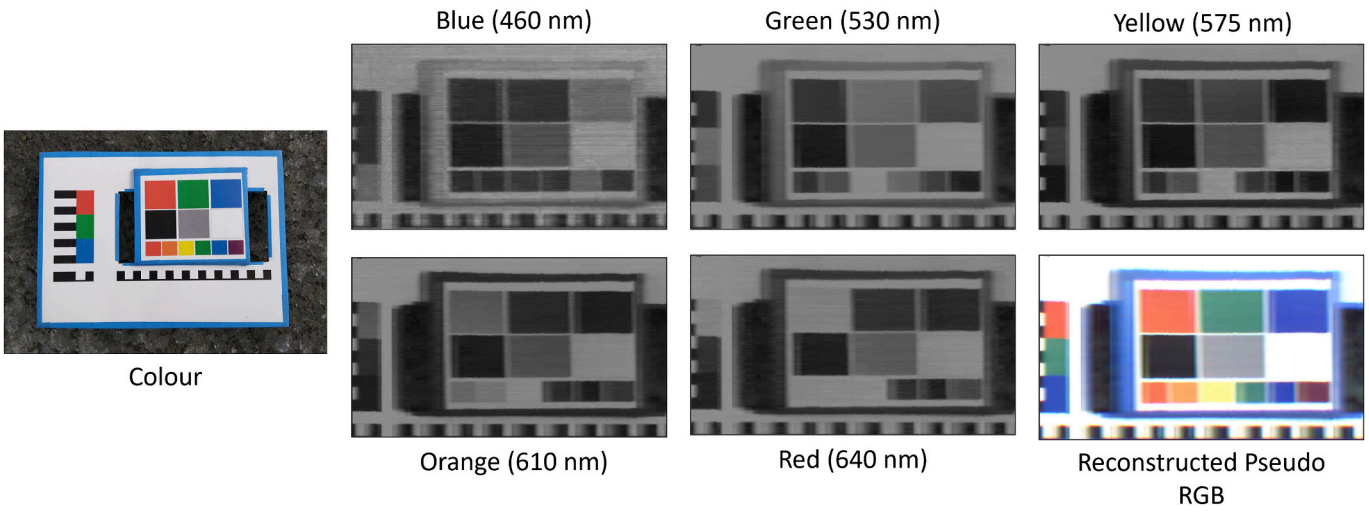

Fig. 3. The test card used for in-field instrument calibration with data cube wavelengths and the reconstructed pseudo RGB image, highlighting the accuracy provided by the instrument.

Table 2
Description of debris samples and their supraglacial locations.

Sample	Description	Site	GPS Coordinates
A	Habitat 1 Debris: Thought to be windblown silt-sized grey clasts	Site i	N 67.15145 W 50.04026
B	Habitat 2 Debris: Thought to be sand and Silt-sized orange/red clasts present within an exposed debris seam	Site ii	N 67.15694 W 50.00383

based on in-field context and analysis. Fig. 4 shows a diagram of the laboratory set-up used for these measurements.

2.6. Snowpack and ice surface energy balance modelling

We acquired hyperspectral images along a glacier transect to demonstrate how the instrumentation could be incorporated into future surface energy balance modelling studies. Sites were located in an approximately southwest-northeast orientation at ca. 50 m elevation intervals (equivalent to 0.2 to 0.7 km apart) from the ice margin towards the main trunk of Isunguata Sermia to a height of 595 m a.s.l. Measured albedo values were calculated for each site and incorporated into the COupled Snowpack and Ice surface energy and mass balance model in PYthon (COSIPY) (Sauter et al., 2020).

We calculated the albedo of supraglacial targets by integrating the spectral intensities of the white portion of the in-scene reference card and the measurand. The albedo was calculated by taking the ratio of these values, using the reference card as a highly diffuse reflective reference surface. The reflectance card provides diffuse reflection across the spectral range of the instruments with a minimum reflectivity of 0.925 at ca. 450 nm. However, before the spectral intensity of the reference card was integrated, the spectral reflectivity of the card had to be calibrated to account for variations resulting from its imperfect spectral reflectance. We measured the spectral reflectivity of the reference card using a Thorlabs spectrometer (CCS200) and integrating sphere (Thorlabs 4P4). A representative sample of the card was placed in the sample port, flush with the interior surface of the sphere, and a broad-spectrum white LED was used for illumination. The spectrometer was coupled to the measuring port of the integrating sphere by a fibre optic and lens (Thorlabs LB1596), the combination of which ensured the field of view of the spectrometer was filled by the sample.

Point simulations of hourly surface melt for each transect location were run using the COSIPY model forced by interpolated data from the KAN_L PROMICE AWS. Atmospheric temperature was interpolated to the elevation of each transect site using a lapse rate of −5.3 °C km^{-1} (Harper et al., 2011). Atmospheric pressure was interpolated using the barometric equation. Hourly total precipitation and snowfall fields were extracted from the nearest ERA5-Land reanalysis grid cell (Muñoz-Sabater et al., 2021). We ran COSIPY for each transect site with both albedo estimates derived from Landsat and Sentinel-2 optical satellite data (Feng et al., 2023) between August 10th - 17th, and those derived from our hyperspectral data.

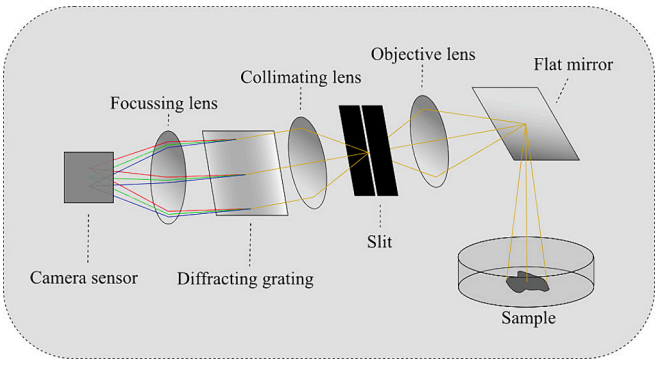

Fig. 4. Experimental set-up used for laboratory measurements of supraglacial debris samples.

3. Results

3.1. Supraglacial measurements

Hyperspectral images were captured across a range of clean ice areas and areas with high concentrations of LAI to test instrument efficacy in a variety of sample collection scenarios. Fig. 5(A) shows a spectral comparison between datasets acquired from clean ice and LAI-covered sites. Clean ice locations show a high intensity response across visible wavelengths, with the greatest intensity present across shorter wavelengths, whereas LAI-covered regions produce a much lower intensity response across all wavelengths. Additionally, this demonstrates that datasets from high albedo locations can be collected with this instrument without encountering problems relating to saturation.

Fig. 5(B) shows the data captured from two visually similar LAI-covered locations. Site i shows Habitat 1 debris, believed to be an area of windblown sediments from local moraine deposits, consisting of silt-sized grey clasts. Site ii shows sediments from Habitat 2, thought to be a

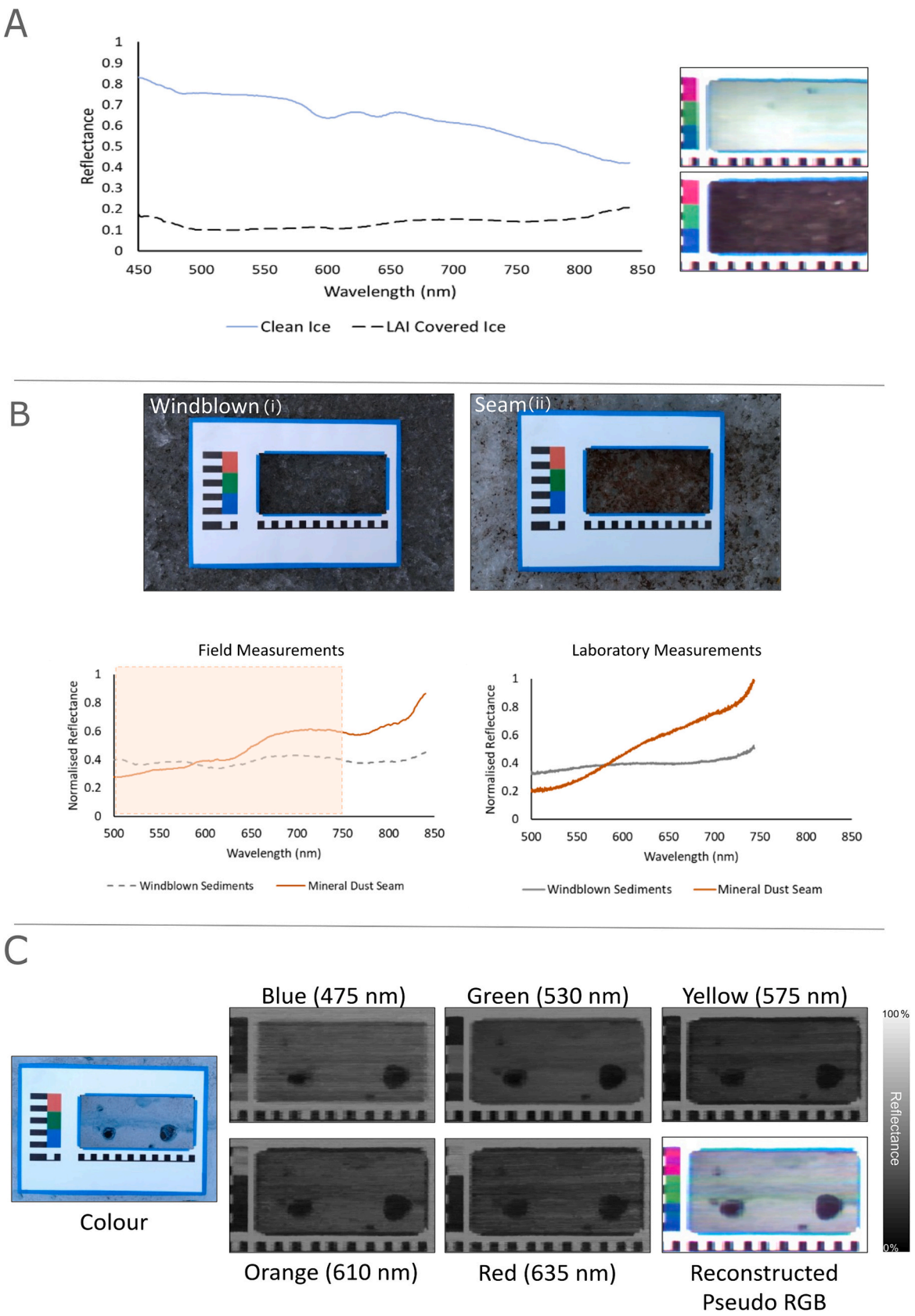

Fig. 5. Supraglacial Measurements. A – spectral datasets for clean ice and LAI-covered locations shown alongside pseudo RGB reconstructions for example locations, albedo values are available in Table 3. B – Comparison of visually similar debris sites. Site i: Habitat 1, Site ii: Habitat 2. Visual datasets of each site are shown alongside their spectral responses recorded in the field and in the laboratory. Highlighted region shows area for direct comparison, emphasising the abilities of our low-cost approach. C – Hyperspectral datasets for a supraglacial location featuring cryoconite holes, demonstrating the instrument's ability to accurately reconstruct on-ice features. Note the target area is defined by the size of the window within the reference card which is ca. 9 cm × 18 cm.

mineral dust seam that is melting out of the ice. These sediments consist of silt and sand-sized red/orange clasts, contrasting with the local deposits (Bøggild et al., 2010; Nagatsuka et al., 2016). Despite these differences, it is clear in Fig. 5(B) that from visual comparisons between the standard photographs, these locations are difficult to distinguish. However, focusing on the spectral information captured from each site, subtle differences between their spectral responses become clear, particularly with the addition of infrared wavelengths. From the spectral data we can differentiate between these two locations, with the debris from the mineral dust seam (Site ii) showing a consistently higher spectral response across orange and red wavelengths (ca. 580 nm – 750 nm).

To further support this analysis, the field data can be directly compared with laboratory analyses of these debris samples. Fig. 5(B) shows the spectral responses of the debris samples captured using the laboratory-based hyperspectral imaging system. These datasets highlight the subtle differences between the samples that can be difficult to identify by eye or with spectral instrumentation with coarser banding. From these data we can clearly identify the increase in spectral response across red wavelengths present in sample ii and the expected low response across all wavelengths in sample i. Residuals were calculated to compare the two measurement systems (laboratory and field) with RMSE = 0.0125 and 0.0249 and R-squared values of 0.991 and 0.973 for windblown sediments and mineral dust seams respectively.

Additionally, a variety of on-ice features were targeted to determine whether these could be accurately identified with the Hyperspectral Smartphone. Fig. 5(C) shows a dataset captured from an area featuring cryoconite holes (typically 5–10 cm diameter cylindrical, water-filled holes in the ice surface created by differential melting of clean ice compared to sediment and biological material (Wharton et al., 1985; Banerjee et al., 2023)) of varying size and depth. This figure demonstrates that these small features can be accurately identified and visually reconstructed using this instrumentation, with cryoconite holes of varying size accurately reconstructed in the hyperspectral data. Note, the banding present in this image is a result of the image capture process.

3.1.1. Albedo measurements

The albedo values calculated from our hyperspectral data and corresponding modelled surface melt vary considerably along the transect (Table 3). There is also significant variability in albedo between nearby sites A4 and A5, despite being less than 100 m apart and at the same elevation. Site A4 has an albedo of 0.44, while site A5 has an albedo of 0.73. This results in a difference in daily surface melt of 1.26 cm w.e. In contrast, using the satellite-derived albedo product, which has a coarser ground footprint, the albedos were very similar (0.58 and 0.60, respectively), leading to a much smaller difference in daily surface melt of 0.09 cm w.e. Overall, there is an increase in albedo away from the margin as is expected because much of the surface darkening in the lower ablation area is predominantly from windblown dust (Wientjes et al., 2011).

At approximately 590 m a.s.l. there is a band of ice with many cryoconite holes. Spatially dense cryoconite holes reduce the albedo calculated using our hyperspectral data because the debris that sits at their bases makes up a significant proportion of the ice surface when viewed from directly overhead. This reduction is not evident in the satellite-derived albedo product (Feng et al., 2023), which is partially derived from off-nadir imagery that does not incorporate cryoconite hole debris due to their high depth-diameter ratio. However, measurements completed by Ryan et al. (2018) found that the presence of cryoconite holes had a minimal impact on albedo, suggesting that our approach may overestimate the impact of cryoconite on albedo in this instance. Overall, our data also show more variability, which is expected given the larger footprint of the satellite-derived albedo data (ca. 100–900 m^2).

3.2. Measurements from the ice sheet foreland

Measurements in the ice sheet foreland were captured from a broad range of targets to better demonstrate the variety of applications that could benefit from the introduction of low-cost hyperspectral imaging approaches. Datasets were collected from a variety of shrub vegetation communities to highlight the accurate detection of spectral features such as pigment variations and red edge increases. Fig. 6(A) shows the spectral responses acquired from two shrub vegetation sites, demonstrating the differences in spectral response between the two vegetation types. Due to the pigmentation of the targets, Arctic Willow (*salix arctica*) shows a higher spectral response across shorter blue/green wavelengths, whereas Bog Bilberry (*vaccinium uliginosum*) shows a marked increase in reflectance across longer orange/red wavelengths. This figure also highlights the benefits provided by the additional NIR wavelengths, enabling red edge detection with a smartphone-based instrument.

Several lichen measurements were also captured. Hyperspectral measurements of lichens have been shown to provide valuable records of species abundance and distribution for lichenometric dating studies as well as an accurate visual record for comparisons with future datasets (Guedes et al., 2022). A variety of crustose lichen species across the ice sheet foreland were imaged using the Hyperspectral Smartphone. Fig. 6 (B) shows a hyperspectral dataset captured from a region of algal growth, thought to be *trentepohlia*, marking a palaeo shoreline of an ice-dammed lake. Lichens such as *rhizocarpon geminatum,* which appear grey in colour, have also begun to colonise the surface. This figure clearly highlights the abilities of the Hyperspectral Smartphone with the reconstructed pseudo RGB dataset accurately portraying the original target.

Table 3
Measurement locations and ice surface information with calculated hyperspectral and satellite-derived albedos for each site.

Name	Date	Latitude (°)	Longitude (°)	Elevation (m a.s.l.)	Surface Type	Hyperspectral		Satellite-Derived Albedo	
						Albedo	Daily SurfaceMelt (cm w.e.)	Albedo	Daily Surface Melt (cm w.e.)
A1	10-Aug 2023	67.15145	−50.0403	490	Wind-blown sediment	0.30	3.60	0.28	3.68
A2	15-Aug 2023	67.15348	−50.0292	493	Wind-blown sediment	0.18	4.11	0.24	3.85
A3	15-Aug 2023	67.15446	−50.0244	496	Mineral dust seam	0.13	4.33	0.33	3.47
A4	15-Aug 2023	67.15581	−50.0172	535	Clean Ice	0.63	2.18	0.39	3.21
A5	15-Aug 2023	67.15969	−50.003	594	Cryoconite features	0.44	3.00	0.58	2.40
A6	10-Aug 2023	67.15911	−50.0034	595	Clean Ice with small cryoconite features	0.73	1.74	0.60	2.31

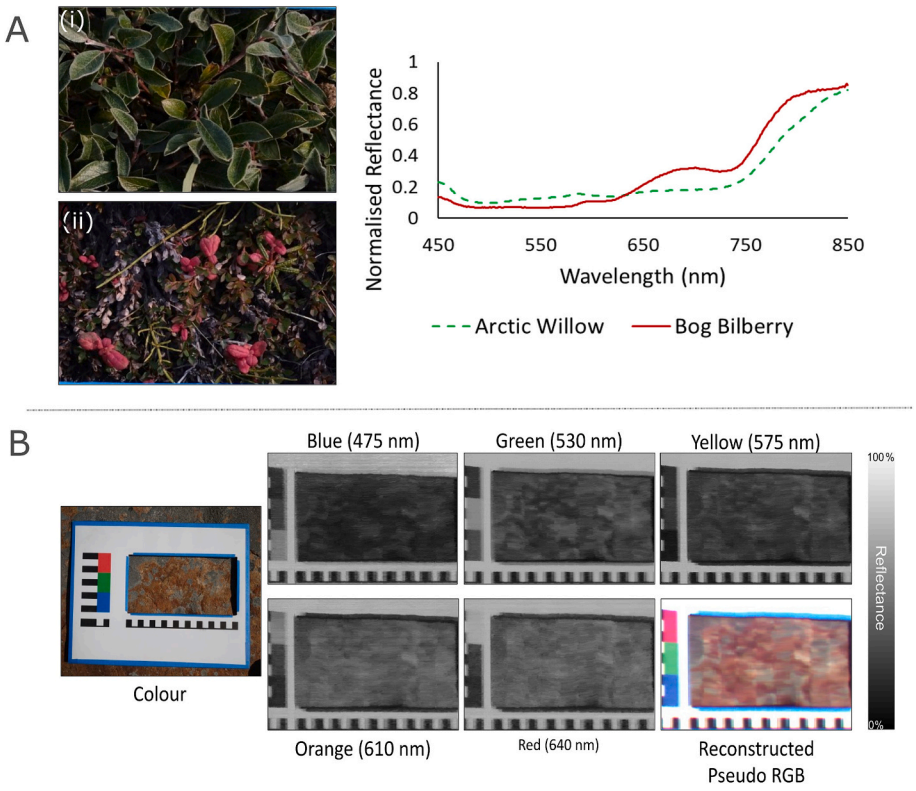

Fig. 6. Proglacial Measurements. A – Spectral comparison of Arctic Willow (i) and Bog Bilberry (ii) highlighting pigment and red edge detection enabled by the extended spectral range. B – Hyperspectral data captured for a region of algal lake staining with grey lichen features. Note the target area is defined by the size of the window within the reference card which is ca. 9 cm × 18 cm.

3.3. Machine learning

Machine learning analysis was applied to several hyperspectral datasets to determine whether target features could be automatically identified across multiple images from their spectral response. The software was trained on example datasets captured with the Hyperspectral Smartphone, with a minimum of five examples provided for each spectral target. Fig. 7(A) shows the results of this process when applied to a supraglacial dataset with multiple cryoconite features. Although cryoconite features are fairly evident in typical visual images, we have included them here to demonstrate that the image segmentation technique can be applied to detect these features, precluding the need for multiple image segmentation techniques. It also serves to provide visual validation for the technique.

This analysis was also applied to proglacial datasets. Fig. 7(B) shows the results obtained from analyses of multiple lichen species. This figure shows that the different lichen species present across the rock surface can be accurately identified from these datasets. Furthermore, the software has also differentiated between areas of lichen and areas of the underlying rock surface, supporting the potential offered by low-cost hyperspectral imaging approaches. Fig. 7(C) further emphasises the success of this approach, showing that areas of lichen can be accurately distinguished from algal targets.

4. Discussion

4.1. Benefits for in-field glacial research

The Hyperspectral Smartphone is an accurate, low-cost alternative to traditional hyperspectral field data collection within the cryosphere. It can provide significant benefits, enabling highly detailed and traditionally expensive hyperspectral datasets to be captured using a portable, low-cost alternative. The light-weight, portable nature of this instrumentation makes it highly suited to applications within the cryosphere, where measurements are often completed in remote locations with uneven/rough terrain. This setting, therefore, makes it difficult to utilise heavier and bulkier instrumentation without encountering significant expenses and/or time-consuming logistics. Increasing data collection opportunities through more accessible instrumentation helps to develop a more detailed picture of the environmental setting. The results above highlight the potential of such instruments for both glacier foreland and supraglacial environments, emphasising their adaptability to different settings and targets within challenging and difficult to access environments.

For supraglacial measurements, the Hyperspectral Smartphone provides a novel means of LAI analysis and identification. Hyperspectral images of the ice surface can be acquired across many sites relatively quickly providing additional information on surface albedo; a key input to surface energy balance models. The results obtained with our instrumentation show similarities to those collected in previous studies e.g. Dal Farra et al. (2018) where the spectral analysis of our sediments produces similar spectral curves. Furthermore, our results agree with previous studies that state that the optical properties of mineral dusts are typically dominated by iron oxides (Kaspari et al., 2014; Zhang et al., 2015; Zhang et al., 2017), resulting in an increase in reflectance across longer wavelengths, which is visible in our datasets. The additional spectral resolution (beyond that captured using standard RGB cameras) enables more accurate identification of different debris types. For example, Ryan et al. (2018), used standard RGB images to identify different surface types, by incorporating our approach it may enable their "distributed impurities" category to be better attributed. Furthermore, we believe, the spectral resolution offered by our approach will enable differentiation between mineral dusts and algal blooms as the absorption features typically associated with snow and ice algae should be visible within the spectral resolution provided by our instrumentation. This could be particularly beneficial when mapping the relative

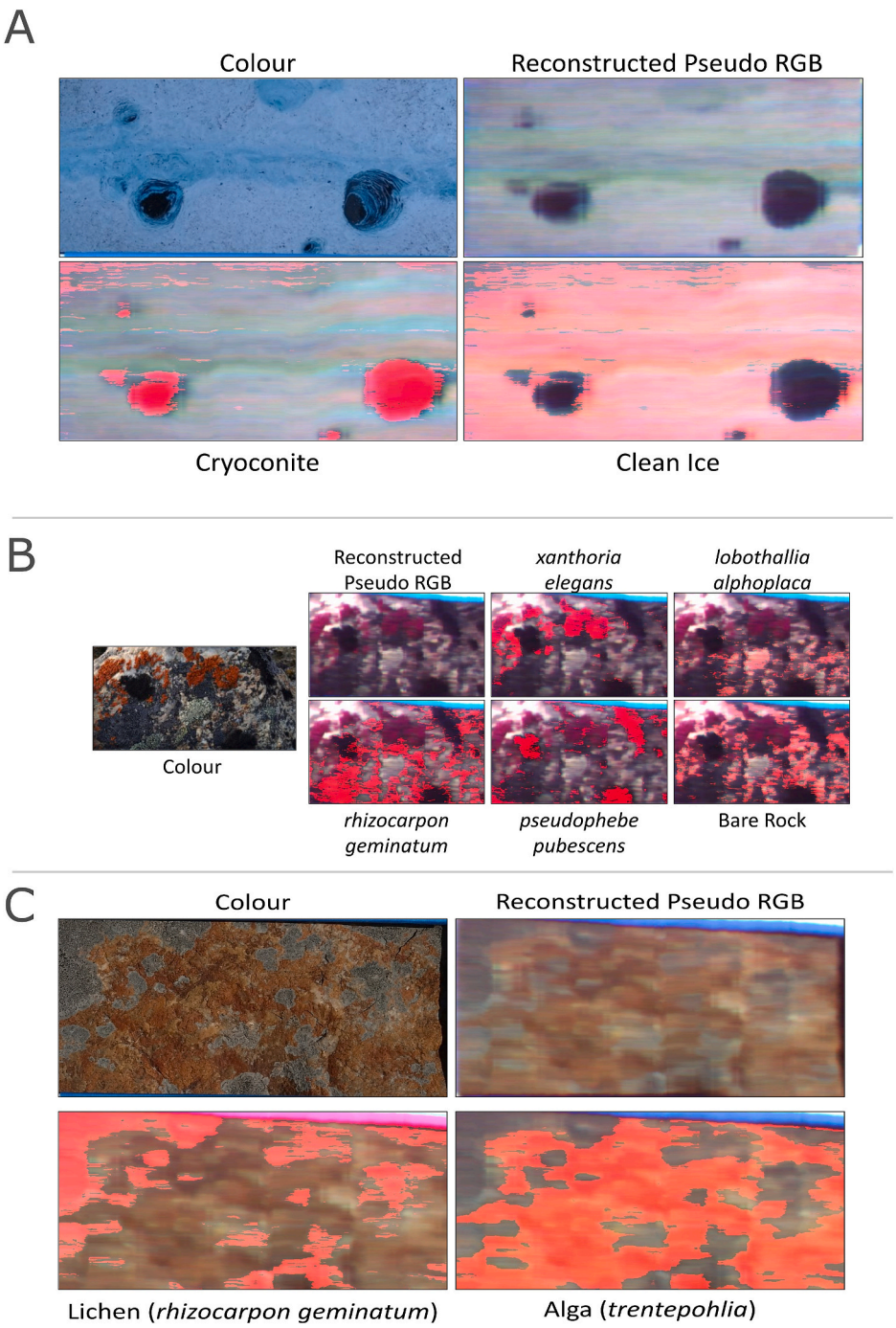

Fig. 7. Machine Learning Applications. Areas highlighted in red indicate the detection of the labelled target. A – Automatic detection of on-ice features. B – Detection and differentiation between different lichen species and the underlying rock surface. C – Detection and differentiation between lichen and lake staining features. Note the target area is defined by the size of the window within the reference card which is ca. 9 cm × 18 cm.

coverage of different debris types, providing a means of identifying their sources. By providing more accessible, highly portable hyperspectral imaging instrumentation, capable of producing datasets that are comparable with current approaches, we can significantly increase the data collection opportunities within these more challenging environmental settings.

There are also considerable opportunities for instrument applications within proglacial settings. The extended spectral range is particularly beneficial, enabling additional information to be obtained from vegetation targets. By including NIR wavelengths within these datasets, vegetation indices such as the Normalised Difference Vegetation Index (NDVI) can be calculated using data captured from a smartphone-based instrument. To date, the measurement of these vegetation indices with smartphones has been infeasible due to the built-in restrictions associated with the camera systems of commercially available units. The introduction of our novel approach, therefore, offers a valuable low-cost alternative to vegetation monitoring studies in these regions. As such, this has considerable potential for applications focusing on Arctic greening and browning (Huete et al., 2002; Brown et al., 2016; Wang and Friedl, 2019; Myers-Smith et al., 2020).

Arctic greening is among the world's most significant large scale ecological responses to climate change (Wang and Friedl, 2019; Myers-

Smith et al., 2020; Shijin and Xiaoqing, 2023). However, its causes and dynamics are complex and remain difficult to measure accurately using existing approaches due to limitations in temporal resolution and poor correlation between datasets captured across different platforms (Myers-Smith et al., 2020). A combined approach, using datasets acquired from satellite, proximal remote sensing, and in-situ measurements, whilst accounting for related scaling issues (Myers-Smith et al., 2020), has been proposed to advance studies of Arctic vegetation change. To be effective this approach will require a significant increase in the temporal resolution of in-situ measurements of Arctic vegetation. The Hyperspectral Smartphone, as a low-cost, rapid, and accurate hyperspectral imaging instrument, could therefore provide a route to improving measurements.

Incorporating the Hyperspectral Smartphone into quantifying vegetation indices would enable a greater number of datasets to be acquired over a wider survey area during the measurement period. Additionally, future developments towards unmanned aerial vehicle (UAV)-mounted surveys with these instruments further increase the measurement opportunities offered. The light-weight nature of these instruments (see Table 1) would allow them to be incorporated within a UAV set-up with relative ease, however, it should be noted that applications involving UAV measurements would require the inclusion of additional optics to ensure reliable data capture over these larger distances.

Low-cost hyperspectral imaging approaches enable the development of high-quality imagery, creating a reliable record of spectral information for a wide variety of targets and locations across the cryosphere. By creating these records, we provide a wealth of data for future analysis and comparison to future datasets without requiring the significant upfront costs associated with many commercial devices. Whilst we acknowledge that standard photographs can act as reliable records for a number of applications, the addition of detailed spectral information provided by hyperspectral instrumentation opens the door to a much wider range of analysis and comparison. These records could prove particularly beneficial within the field of lichenometry, for example, where current measurement approaches can often be subjective and lacking in visual records that enable accurate comparisons between datasets (Guedes et al., 2022). Hyperspectral datasets enable the identification of specific spectral signatures, providing a more robust means of differentiating between species, reducing the potential for the misidentification of vegetation and lichen species.

Finally, the successful application of machine learning analysis techniques to these datasets demonstrates the level of detail, and quantitative information that can be extracted using this low-cost instrumentation. The reliable identification of, and distinction between, the spectral characteristics of targets provides access to a wealth of information that was difficult to acquire hitherto. Combining these techniques within a low-cost, more accessible approach provides a path towards increasing our understanding of the processes influencing these key environmental settings whilst also bringing us closer to the democratisation of these valuable analytical techniques within the cryosphere.

4.2. Practicalities for field deployment

The above sections highlight the considerable potential offered by the outputs of the Hyperspectral Smartphone. This section aims to provide an insight into the practicalities of deploying this instrumentation within an Arctic field setting. Some of the greatest challenges faced by instrument applications in these environments are portability and power consumption, with typical commercial instruments being large, and bulky with significant power requirements. In contrast, the Hyperspectral Smartphone is highly portable requiring only a smartphone equipped with the spectral housing, and the in-scene reference card to enable accurate in-field data collection. As such, these instruments can be carried with ease in hand luggage, minimising their impact on trip logistics. in the field, these pieces of equipment can be carried in a rucksack alongside other field equipment, as demonstrated within this study where the instruments were transported to the field sites daily in this manner without encountering any problems or breakages. This enables the user to capture a broad range of datasets across multiple locations without considerable set-up times or acquisition periods. Furthermore, the only power requirements are those of the smartphones themselves which were charged at the field camp with a small solar panel prior to deployment for data capture, removing the need for the transport of large battery power supplies.

The battery life offered by these instruments is also significant, with both instruments requiring only two charges over the two-week research period. Whilst we acknowledge that colder measurement conditions or more intense surveys will likely reduce battery life considerably, the instruments are small enough that they could easily be placed inside a jacket to keep them warm until they are needed for measurements. For longer deployments a small power bank could be carried to provide several phone charges. Additionally, data acquisition is rapid with scans taking ca. 10 s to complete. This offers a considerable improvement on existing approaches which typically take over 10 min to successfully collect a dataset. Whilst there are snapshot-style approaches that enable data acquisition times similar to those offered by the Hyperspectral Smartphone, these instruments cost more than £20,000, which is over an order of magnitude more expensive than our smartphone-based approach.

5. Conclusions

In this article we have applied a smartphone-based hyperspectral imaging instrument and machine learning techniques to data collection and analysis activities at Isunguata Sermia, south-west Greenland. Our results demonstrate the substantial potential offered by hyperspectral imaging techniques, indicating that the limitations often associated with low-cost components are now being overcome as technologies continue to improve and develop. The datasets captured by these instruments are similar to those found by other studies, despite being captured on devices that cost over an order of magnitude less than typical commercially available systems. The applications demonstrated in this article represent a small number of measurement opportunities available within more extreme environmental settings, with the introduction of accurate and reliable low-cost hyperspectral imaging alternatives unlocking a wealth of data collection opportunities that were hitherto infeasible. These new approaches, therefore, provide a significant step towards the democratisation of this valuable analytical technique, helping to improve our understanding of a wide range of more difficult to access environmental settings.

Funding

This research received no external funding.

CRediT authorship contribution statement

M.B. Stuart: Writing – review & editing, Writing – original draft, Validation, Resources, Project administration, Methodology, Investigation, Formal analysis, Data curation, Conceptualization. **M. Davies:** Writing – review & editing, Validation, Software, Investigation, Data curation. **C. Fisk:** Writing – review & editing, Software. **E. Allen:** Writing – review & editing, Resources. **A.J. Sole:** Writing – review & editing, Data curation. **R. Ing:** Writing – review & editing, Formal analysis. **M.J. Hobbs:** Writing – review & editing. **J.R. Willmott:** Writing – review & editing, Resources.

Declaration of competing interest

The authors declare that they have no known competing financial interests or personal relationships that could have appeared to influence the work reported in this paper.

Data availability

Data will be made available on request.

Acknowledgements

The authors would like to thank PyrOptik Instruments Ltd. for use of their prototype ChromaMapper technology, and the students of the 2023 University of Sheffield Polar and Alpine Change MSc (Res) course for their interest in this project and their support during the field work.

References

Aasen, H., Burkart, A., Bolten, A., Bareth, G., 2015. Generating 3D hyperspectral information with lightweight UAV snapshot cameras for vegetation monitoring: from camera calibration to quality assurance. ISPRS J. Photogramm. Remote Sens. 108, 245–259. https://doi.org/10.1016/j.isprsjprs.2015.08.002.

Banerjee, A., Sarangi, C., Rashid, I., Vijay, S., Najar, N.A., Chandel, A.S., 2023. A scaling relation for Cryoconite holes. Geophys. Res. Lett. 50 (22) https://doi.org/10.1029/2023GL104942.

Bartholomew, I.D., Nienow, P., Sole, A., Mair, D., Cowton, T., King, M.A., Palmer, S., 2011. Seasonal variations in Greenland ice sheet motion: inland extent and behaviour at higher elevations. Earth Planet. Sci. Lett. 307 (3–4), 271–278. https://doi.org/10.1016/j.epsl.2011.04.014.

Bøggild, C.E., Brandt, R.E., Brown, K.J., Warren, S.G., 2010. The ablation zone in Northeast Greenland: ice types, albedos and impurities. J. Glaciol. 56 (195), 101–113. https://doi.org/10.3189/002214310791190776.

Brown, T.B., Hultine, K.R., Steltzer, H., Denny, E.G., Denslow, M.W., Granados, J., Henderson, S., Moore, D., Nagai, S., Sanclements, M., Sánchez-Azofeifa, A., Sonnentag, O., Tazik, D., Richardson, A.D., 2016. Using phenocams to monitor our changing earth: toward a global phenocam network. Front. Ecol. Environ. 14 (2), 84–93. https://doi.org/10.1002/fee.1222.

Casey, K., Kääb, A., 2012. Estimation of supraglacial dust and debris geochemical composition via satellite reflectance and emissivity. Remote Sens. 4 (9), 2554–2575. https://doi.org/10.3390/rs4092554.

Cook, J.M., Hodson, A.J., Gardner, A.S., Flanner, M., Tedstone, A.J., Williamson, C., Irvine-Fynn, T.D., Nilsson, J., Bryant, R., Tranter, M., 2017a. Quantifying bioalbedo: a new physically-based model and critique of empirical methods for characterizing biological influence on ice and snow albedo. Cryosphere 1875, 1–29. https://doi.org/10.5194/tc-2017-73.

Cook, J.M., Hodson, A.J., Taggart, A.J., Mernild, S.H., Tranter, M., 2017b. A predictive model for the spectral "bioalbedo" of snow. J. Geophys. Res. Earth 122 (1), 434–454. https://doi.org/10.1002/2016JF003932.

Dal Farra, A., Kaspari, S., Beach, J., Bucheli, T.D., Schaepman, M., Schwikowski, M., 2018. Spectral signatures of submicron scale light-absorbing impurities in snow and ice using hyperspectral microscopy. J. Glaciol. 64 (245), 377–386. https://doi.org/10.1017/jog.2018.29.

Davies, M., Stuart, M.B., Hobbs, M.J., McGonigle, A.J.S., Willmott, J.R., 2022. Image correction and in-situ spectral calibration for low-cost, smartphone hyperspectral imaging. Remote Sens. 14, 1152. https://doi.org/10.3390/rs14051152.

Derkacheva, A., Gillet-Chaulet, F., Mouginot, J., Jager, E., Maier, N., Cook, S., 2021. Seasonal evolution of basal environment conditions of Russell sector, West Greenland, inverted from satellite observation of surface flow. Cryosphere 15 (12), 5675–5704. https://doi.org/10.5194/tc-15-5675-2021.

Di Mauro, B., Baccolo, G., Garzonio, R., Giardino, C., Massabò, D., Piazzalunga, A., Rossini, M., Colombo, R., 2017. Impact of impurities and cryoconite on the optical properties of the Morteratsch glacier (Swiss Alps). Cryosphere 11 (6), 2393–2409. https://doi.org/10.5194/tc-11-2393-2017.

Di Mauro, B., Fava, F., Ferrero, L., Garzonio, R., Baccolo, G., Delmonte, B., & Colombo, R. (2015). Mineral dust impact on snow radiative propertiesin the European Alps combining ground, UAV,and satellite observations. Nature, 120, 6080–6097. DOI:https://doi.org/10.1038/175238c0.

Dumont, M., Brun, E., Picard, G., Michou, M., Libois, Q., Petit, J.R., Geyer, M., Morin, S., Josse, B., 2014. Contribution of light-absorbing impurities in snow to Greenland's darkening since 2009. Nat. Geosci. 7 (7), 509–512. https://doi.org/10.1038/ngeo2180.

Fausto, R.S., van As, D., Mankoff, K.D., Vandecrux, B., Citterio, M., Ahlstrøm, A.P., Andersen, S.B., Colgan, W., Karlsson, N.B., Kjeldsen, K.K., Korsgaard, N.J., Larsen, S. H., Nielsen, S., Pedersen, A.Ø., Shields, C.L., Solgaard, A.M., Box, J.E., 2021. Programme for monitoring of the Greenland ice sheet (PROMICE) automatic weather station data. Earth System Science Data 13 (8), 3819–3845. https://doi.org/10.5194/essd-13-3819-2021.

Feng, S., Cook, J.M., Anesio, A.M., Benning, L.G., Tranter, M., 2023. Long time series (1984-2020) of albedo variations on the Greenland ice sheet from harmonized Landsat and sentinel 2 imagery. J. Glaciol. 6 (4) https://doi.org/10.1017/jog.2023.11.

Guedes, P., Oliveira, M.A., Branquinho, C., Silva, J.N., 2022. Image analysis for automatic measurement of crustose lichens. arXiv preprint arXiv 2203.00787.

Halbach, L., Chevrollier, L.-A., Cook, J.M., Stevens, I.T., Hansen, M., Anesio, A.M., Benning, L.G., Tranter, M., 2023. Dark ice in a warming world: advances and challenges in the study of Greenland ice Sheet's biological darkening. Ann. Glaciol. 1–6 https://doi.org/10.1017/aog.2023.17.

Harper, J., Hubbard, A., Ruskeeniemi, T., Claesson Liljedahl, L., Lehtinen, A., Booth, A., Brinkerhoff, D., Drake, H., Dow, C., Doyle, S., Engström, J., Fitzpatrick, A., Frape, S., Henkemans, E., Humphrey, N., Johnson, J., Jones, G., Joughin, I., Klint, K., Kukkonen, I., Kulessa, B., Landowski, C., Lindbäck, K., Makahnouk, M., Meierbachtol, T., Pere, T., Pedersen, K., Pettersson, R., Pimentel, S., Quincey, D., Tullborg, E.-L., van As, D., 2011. The Greenland Analogue Project Yearly Report 2010.

Harper, J., Meierbachtol, T., Humphrey, N., Saito, J., Stansberry, A., 2021. Variability of Basal Meltwater Generation during Winter. The Cryosphere, Western Greenland Ice Sheet. https://doi.org/10.5194/tc-2021-179.

Huete, A., Didan, K., Miura, T., Rodriguez, E.P., Gao, X., Ferreira, L.G., 2002. Overview of the radiometric and biophysical performance of the MODIS vegetation indices. Remote Sens. Environ. 83, 195–213. https://doi.org/10.1016/S0034-4257(02)00096-2.

Jia, J., Wang, Y., Chen, J., Guo, R., Shu, R., Wang, J., 2020. Status and application of advanced airborne hyperspectral imaging technology: a review. Infrared Phys. Technol. 104, 103115 https://doi.org/10.1016/j.infrared.2019.103115.

Jones, C., Ryan, J., Holt, T., Hubbard, A., 2018. Structural glaciology f Isunguata Sermia. West Greenland. *J. Maps* 14 (2), 517–527. https://doi.org/10.1080/17445647.2018.1507952.

Kaspari, S., Painter, T.H., Gysel, M., Skiles, S.M., Schwikowski, M., 2014. Seasonal and elevational variations of black carbon and dust in snow and ice in the Solu-Khumbu, Nepal and estimated radiative forcings. Atmos. Chem. Phys. 14, 8089–8103. https://doi.org/10.5194/acp-14-8089-2014.

Lindbäck, K., Pettersson, R., 2015. Spectral roughness and glacial erosion of a land-terminating section of the Greenland ice sheet. Geomorphology 238, 149–159. https://doi.org/10.1016/j.geomorph.2015.02.027.

Maier, N., Humphrey, N., Harper, J., Meierbachtol, T., 2019. Sliding dominates slow-flowing margin regions, Greenland ice sheet. *Science*. Advances 5 (7). https://doi.org/10.1126/sciadv.aaw5406.

Muñoz-Sabater, J., Dutra, E., Agustí-Panareda, A., Albergel, C., Arduini, G., Balsamo, G., Boussetta, S., Choulga, M., Harrigan, S., Hersbach, H., Martens, B., Miralles, D.G., Piles, M., Rodríguez-Fernández, N.J., Zsoter, E., Buontempo, C., Thépaut, J.-N., 2021. ERA5-land: a state-of-the-art global reanalysis dataset for land applications. Earth System Science Data 13 (9), 4349–4383. https://doi.org/10.5194/essd-13-4349-2021.

Myers-Smith, I.H., Kerby, J.T., Phoenix, G.K., Bjerke, J.W., Epstein, H.E., Assmann, J.J., John, C., Andreu-Hayles, L., Angers-Blondin, S., Beck, P.S.A., Berner, L.T., Bhatt, U. S., Bjorkman, A.D., Blok, D., Bryn, A., Christiansen, C.T., Cornelissen, J.H.C., Cunliffe, A.M., Elmendorf, S.C., Forbes, B.C., Goetz, S.J., Hollister, R.D., de Jong, R., Loranty, M.M., Macias-Fauria, M., Maseyk, K., Normand, S., Olofsson, J., Parker, T. C., Parmentier, F.-J.W., Post, E., Schaepman-Strub, G., Stordal, F., Sullivan, P.F., Thomas, H.J.D., Tømmervik, H., Treharne, R., Tweedie, C.E., Walker, D.A., Wilmking, M., Wipf, S., 2020. Complexity revealed in the greening of the Arctic. Nat. Clim. Chang. 10 (2), 106–117. https://doi.org/10.1038/s41558-019-0688-1.

Naegeli, K., Damm, A., Huss, M., Schaepman, M., Hoelzle, M., 2015. Imaging spectroscopy to assess the composition of ice surface materials and their impact on glacier mass balance. Remote Sens. Environ. 168, 388–402. https://doi.org/10.1016/j.rse.2015.07.006.

Nagatsuka, N., Takeuchi, N., Uetake, J., Shimada, R., Onuma, Y., Tanaka, S., Nakano, T., 2016. Variations in Sr and Nd isotopic ratios of mineral particles in cryoconite in western Greenland. Front. Earth Sci. 4 https://doi.org/10.3389/feart.2016.00093.

Näsi, R., Honkavaara, E., Lyytikäinen-Saarenmaa, P., Blomqvist, M., Litkey, P., Hakala, T., Tanhuanpää, T., Holopainen, M., 2015. Using UAV-based photogrammetry and hyperspectral imaging for mapping bark beetle damage at tree-level. Remote Sens. 7, 15467–15493. https://doi.org/10.3390/rs71115467.

O'Neal, M.A., 2010. Identifying lichenometrically datable, glacierized terrains: a case study in the cascade range of Western North America. Geocarto Int. 25 (4), 315–325. https://doi.org/10.1080/10106040903362836.

Painter, T.H., Duval, B., Thomas, W.H., Mendez, M., Heintzelman, S., Dozier, J., 2001. Detection and quantification of snow algae with an airborne imaging spectrometer. Appl. Environ. Microbiol. 67 (3−12), 5267–5272. https://doi.org/10.1128/aem.67.11.5267-5272.2001.

Palmer, S., Shepherd, A., Nienow, P., Joughin, I., 2011. Seasonal speedup of the Greenland ice sheet linked to routing of surface water. Earth Planet. Sci. Lett. 302 (3–4), 423–428. https://doi.org/10.1016/j.epsl.2010.12.037.

Patmanee, J., Pinthong, C., Kanprachar, S., 2024. Estimation of suitable low-frequency passbands of MMFs using neural network. In: 2024 21st International Conference on Electrical Engineering/Electronics, Computer, Telecommunications and Information Technology (ECTI-CON). Khon Kaen, Thailand, pp. 1–6. https://doi.org/10.1109/ECTI-CON60892.2024.10594965.

Rodrigues, E.M., Hemmer, E., 2022. Trends in hyperspectral imaging: from environmental and health sensing to structure-property and nano-bio interaction studies. Anal. Bioanal. Chem. 414, 4269–4279. https://doi.org/10.1007/s00216-022-03959-y.

Ryan, J.C., Hubbard, A., Stibal, M., Irvine-Fynn, T.D., Cook, J., Smith, L.C., Cameron, K., Box, J., 2018. Dark zone of the Greenland ice sheet controlled by distributed biologically-active impurities. Nat. Commun. 9, 1065. https://doi.org/10.1038/s41467-018-03353-2.

Salehi, S., Karami, M., Fensholt, R., 2016. Identification of a robust lichen index for the deconvolution of lichen and rock mixtures using pattern search algorithm (case study: Greenland). International Archives of the Photogrammetry, Remote Sensing and Spatial Information Sciences - ISPRS Archives 41, 973–979. https://doi.org/10.5194/isprsarchives-XLI-B7-973-2016.

Sauter, T., Arndt, A., Schneider, C., 2020. COSIPY v1.3 – an open-source coupled snowpack and ice surface energy and mass balance model. Geosci. Model Dev. 13 (11), 5645–5662. https://doi.org/10.5194/gmd-13-5645-2020.

Seager, S., Turner, E.L., Schafer, J., Ford, E.B., 2005. Vegetation's Red Edge: A Possible Spectroscopic Biosignature of Extraterrestrial Plants. https://doi.org/10.1089/ast.2005.5.372.

Shijin, W., Xiaoqing, P., 2023. Permafrost degradation services for Arctic greening. Catena 229. https://doi.org/10.1016/j.catena.2023.107209.

Slightam, J.E., Griego, A.D., 2023. Deep neural network design for improving stability and transient behaviour in impedance control applications. In: *2023 IEEE/ASME International Conference on Advanced Intelligence Mechatronics (AIM),* Seattle, WA, USA, pp. 1336–1343. https://doi.org/10.1109/AIM46323.2023.10196286.

Sole, A., Nienow, P., Bartholomew, I., Mair, D., Cowton, T., Tedstone, A., King, M.A., 2013. Winter motion mediates dynamic response of the Greenland ice sheet to warmer summers. Geophys. Res. Lett. 40 (15), 3940–3944. https://doi.org/10.1002/grl.50764.

Stuart, M.B., Davies, M., Hobbs, M.J., McGonigle, A.J.S., Willmott, J.R., 2022a. Peatland plant spectral response as a proxy for peat health, analysis using low-cost hyperspectral imaging techniques. Remote Sens. 14 (16) https://doi.org/10.3390/rs14163846.

Stuart, M.B., Davies, M., Hobbs, M.J., Pering, T.D., McGonigle, A.J.S., Willmott, J.R., 2022b. High-resolution hyperspectral imaging using low-cost components: application within environmental monitoring scenarios. Sensors 22 (12). https://doi.org/10.3390/s22124652.

Stuart, M.B., McGonigle, A.J.S., Davies, M., Hobbs, M.J., Boone, N.A., Stanger, L.R., Zhu, C., Pering, T.D., Willmott, J.R., 2021. Low-cost hyperspectral imaging with a smartphone. Journal of Imaging 7 (8), 1–13. https://doi.org/10.3390/jimaging7080136.

Stuart, M.B., McGonigle, A.J.S., Willmott, J.R., 2019. Hyperspectral imaging in environmental monitoring: a review of recent developments and technological advances in compact field deployable systems. Sensors (Switzerland) 19 (14). https://doi.org/10.3390/s19143071.

Van De Wal, R.S.W., Boot, W., Smeets, C.J.P.P., Snellen, H., Van Den Broeke, M.R., Oerlemans, J., 2012. Twenty-one years of mass balance observations along the K-transect. West Greenland. Earth System Science Data 4 (1), 31–35. https://doi.org/10.5194/essd-4-31-2012.

Van der Veen, C.J., Csatho, B.M., 2005. Spectral characteristics of Greenland lichens. Géog. Phys. Quatern. 59 (1), 63–73. https://doi.org/10.7202/013737ar.

Wang, J.A., Friedl, M.A., 2019. The role of land cover change in Arctic-boreal greening and browning trends. Environ. Res. Lett. 14 (12) https://doi.org/10.1088/1748-9326/ab5429.

Wang, S., Tedesco, M., Alexander, P., Xu, M., Fettweis, X., 2020. Quantifying spatiotemporal variability of glacier algal blooms and the impact on surface albedo in southwestern Greenland. Cryosphere 14 (8), 2687–2713. https://doi.org/10.5194/tc-14-2687-2020.

Warren, S.G., 2019. Light-absorbing impurities in snow: a personal and historical account. Front. Earth Sci. 6, 250. https://doi.org/10.3389/feart.2018.00250.

Wharton, R.A., Mckay, C.P., Simmons, G.M., Parker, B.C., 1985. Cryoconite holes on glaciers. Bioscience 35 (8), 499–503. https://doi.org/10.2307/1309818.

Wientjes, I.G.M., Van De Wal, R.S.W., Reichart, G.J., Sluijs, A., Oerlemans, J., 2011. Dust from the dark region in the western ablation zone of the Greenland ice sheet. Cryosphere 5 (3), 589–601. https://doi.org/10.5194/tc-5-589-2011.

Williamson, C.J., Cameron, K.A., Cook, J.M., Zarsky, J.D., Stibal, M., Edwards, A., 2019. Glacier algae: a dark past and a darker future. Front. Microbiol. 10, 436973 https://doi.org/10.3389/fmicb.2019.00524.

Wright, P.J., Harper, J.T., Humphrey, N.F., Meierbachtol, T.W., 2016. Measured basal water pressure variability of the western Greenland ice sheet: implications for hydraulic potential. J. Geophys. Res. Earth 121 (6), 1134–1147. https://doi.org/10.1002/2016JF003819.

Yde, J.C., Anderson, N.J., Post, E., Saros, J.E., Telling, J., 2018. Environmental change and impacts in the Kangerlussuaq area, West Greenland. Arct. Antarct. Alp. Res. 50 (1) https://doi.org/10.1080/15230430.2018.1433786.

Zhang, X.L., Wu, G.J., Zhang, C.L., Xu, T.L., Zhou, Q.Q., 2015. What is the real role of iron oxides in the optical properties of dust aerosols? Atmos. Chem. Phys. 15, 12159–12177. https://doi.org/10.5194/acp-15-12159-2015.

Zhang, Y., Kang, S., Cong, Z., Schmale, J., Sprenger, M., Li, C., Yang, W., Gao, T., Sillanpää, M., Li, X., Liu, Y., Chen, P., Zhang, X., 2017. Light-absorbing impurities enhance glacier albedo reduction in the southeastern Tibetan plateau. J. Geophys. Res. 122 (13), 6915–6933. https://doi.org/10.1002/2016JD026397.